

Entropy and Barrier-Hopping Determine Conformational Viscoelasticity in Single Biomolecules

Bhavin S. Khatri, Masaru Kawakami, Katherine Byrne,
D. Alastair Smith, Tom C.B. McLeish,*

¹*Institute of Molecular Biophysics & Polymer and Complex Fluids Group, School of Physics and Astronomy, University of Leeds, Leeds LS2 9JT, UK*

Biological macromolecules have complex and non-trivial energy landscapes, endowing them a unique conformational adaptability and diversity in function. Hence, understanding the processes of elasticity and dissipation at the nanoscale is important to molecular biology and also emerging fields such as nanotechnology. Here we analyse single molecule fluctuations in an atomic force microscope (AFM) experiment using a generic model of biopolymer viscoelasticity that importantly includes sources of local ‘internal’ conformational dissipation. Comparing two biopolymers, dextran and cellulose, polysaccharides with and without the well-known ‘chair-to-boat’ transition, reveals a signature of this simple conformational change as minima in both the elasticity and internal friction around a characteristic force. A calculation of two-state populations dynamics offers a simple explanation in terms of an elasticity driven by the entropy, and friction by barrier-controlled hopping, of populations on a landscape. The microscopic model, allows quantitative mapping of features of the energy landscape, revealing unexpectedly slow dynamics, suggestive of an underlying roughness to the free energy.

The paradigm underlying many force probe experiments is the linear increase of tensile force on a single biomolecule with time¹. An emergent theme from constant loading rate experiments is the propensity for conformational change in biomolecules, from reversible processes such as chair-boat transitions in polysaccharides²⁻⁵ and the overstretching transition in DNA⁶⁻⁸ to the irreversible unfolding of concatamers of protein domains⁹⁻¹⁴. In addition, conformational transitions are ubiquitous in biological processes; for example, static and dynamic changes in structure are known to be important in many signalling processes in molecular biology¹⁵. However despite their importance, the physical processes that underly these transitions, in particular the role of conformational elasticity and internal friction, are poorly understood.

Despite the success of constant loading rate experiments, they can provide only limited information; the elastic response function for each molecule under reversible conditions, and at most *global* dynamical information, such as the rate of unfolding of a protein, from irreversible stretching. A case in point is the polysaccharide dextran, which exhibits a reversible plateau in its force-extension response, due to a local chair-boat transition that has been shown to be two-state in nature^{5,16}. Such experiments provide the free energy difference and distance between states, however, the dynamics of this transition are too fast for stretching experiments to probe. A fuller understanding of the response of single biopolymers during forced unfolding or refolding could be provided by analysis of the *local* linear viscoelastic response. Significantly, local dissipation would give access to finer-scale conformational dynamics, for example, the rates of transitions between different states along the unfolding or refolding pathways of a protein. A close analogy is found in the macroscopic rheology of complex fluids, whose dissipative mechanical spectra reflect dynamics of various structural, molecular and topological transitions¹⁷.

Recent experiments¹⁸⁻²⁵ measuring the viscoelastic properties of single biomolecules as a function of force, including polysaccharides and proteins, have gone some way to achieving this goal. The results show highly non-trivial features, particularly in the dissipative part of the spectra, where measured frictions are many orders of magnitude larger than that due to solvent. In particular, the friction of dextran exhibits a minimum at a force that coincides with the plateau in the force-extension trace, indicating it arises through a process related to the local conformational transitions in the chain^{18,24}. In addition, although it is clear that a plateau in the force-extension response, should give rise to a minimum in elasticity, the underlying statistical mechanics of this change are not well understood^{2,3}. Here we seek to understand the origins of these features in the viscoelasticity of dextran and by doing so give broad insight to the nature of elasticity and friction

for simple conformational transitions.

Dextran and cellulose are polysaccharides that are biological polymers composed of glucose monomers, a six-membered ring molecule, which is known to have a number of stable conformations²⁶ (Fig.1). These biopolymers differ by the way the glucose ring is linked into the backbone of the polymer. In dextran, one of the linkages is axial to the plane of the ring and thus force promotes conversion from the nominally stable chair state to a more elongated boat-like conformation, in which this linkage is equatorial²⁷, as shown in Fig.1a. This gives rise to dextran’s characteristic plateau in its force extension response (Appendix: Fig.1). In contrast, the glucose ring in cellulose is already near maximum elongation since all its linkages are equatorial to the plane of the ring (Fig.1b) and results in almost ideal freely jointed chain (FJC) properties in its force-extension response^{3,4} (Appendix: Fig.7). Hence, we will show through the experimental comparison of the viscoelasticity of these two polysaccharides, that the two-state nature of the transition in dextran and its absence in cellulose, provides an ideal test-bed to understand the characteristic viscoelastic response of simple forced conformational transitions.

We determine the viscoelasticity of dextran and cellulose, using a recently developed technique for measuring the Brownian dynamics of single molecules under force-clamp conditions²⁴. Fig.2a summarises the experimental apparatus and procedure, with details given in Methods. The principle of the experiment is to hold a single molecule between tip and substrate of an AFM at constant force, whilst observing the thermal fluctuations of the cantilever. The fluctuations contain inherent viscoelastic information, which we obtain via calculation of their frequency power spectral density (PSD). A conventional proportional-integral-derivative (PID) feedback loop with a response time of ~ 10 ms, monitors the cantilever deflection signal and adjusts the piezo substrate to maintain a constant average force (F) or “force-clamp” on the molecule between the tip and substrate. A key idea of this technique is that by controlling the force we probe the local viscoelasticity of single biomolecules as they explore their energy landscape under near equilibrium conditions. Measurement of the force-dependent power spectra is exemplified in Fig.3 for cellulose, where it is clear that the PSD peak position, width and amplitude are dependent on the response of the biopolymer.

To quantify these changes and extract viscoelastic information from the thermal spectroscopy power spectra, we model the biopolymer using a modified Rouse model that includes local conformational internal friction, in addition to solvent friction^{28,29}. The Rouse model is a generic and

highly successful description of the coarse-grained dynamical behaviour of polymers^{30,31}, where we note that in the typically highly extended conformations in our experiment, long-range hydrodynamics³² give only logarithmic corrections to local drag. The Rouse with Internal Friction (RIF) polymer is represented as a series of beads with solvent friction ζ_{s0} , connected by spring and dashpots of elasticity κ_0 and internal friction ζ_{i0} . In the continuum limit, internal friction adds an extra term in the standard Rouse equation, which describes a dissipative force proportional to the rate of change of local conformation, represented as the coarse-grained curvature of the chain,

$$\zeta_{s0} \frac{\partial \mathbf{R}(n, t)}{\partial t} = \left(\kappa_0 + \zeta_{i0} \frac{\partial}{\partial t} \right) \frac{\partial^2 \mathbf{R}(n, t)}{\partial n^2} + \mathbf{f}(n, t), \quad (1)$$

where $\mathbf{R}(n, t)$ represents the space curve of the polymer with contour variable n , subject to a local Langevin force $\mathbf{f}(n, t)$, which is uncorrelated for different times. Normal mode solutions of this equation decay in a single exponential manner with a mode dependent relaxation time, $\tau_p = \frac{N\zeta_p}{2\pi^2\kappa_0 p^2}$, where p is the mode number. the effective mode friction is renormalised compared to standard Rouse theory to $\zeta_p = 2N\zeta_{s0} + \frac{2\pi^2 p^2 \zeta_{i0}}{N}$, where intuitively, the new term accounts for an increasing internal friction of higher curvature short wavelength modes. AFM experiments probe the end-to-end vector of the polymer, whose response can be found by summing over all odd modes; in frequency space this gives the following useful closed form expression for the dynamic compliance:

$$J_{\Delta R}(\omega) = \frac{2N}{\pi\kappa_0} \frac{\tanh\left(\frac{\pi}{2} \sqrt{\frac{i\omega\tau_R}{1+i\omega\tau_i}}\right)}{\sqrt{i\omega\tau_R(1+i\omega\tau_i)}}, \quad (2)$$

where $\tau_R = N^2\zeta_{s0}/\pi^2\kappa_0$ is the contribution to the relaxation time of the first mode due to solvent friction and $\tau_i = \zeta_{i0}/\kappa_0$ is the mode-independent contribution to the relaxation time due to internal friction. This model successfully encompasses the behaviour of both types of friction; in the limit of large internal friction ($\tau_R \ll \tau_i$), Eq.(2) reduces to a single mode spring and dashpot model, $J_{\Delta R}(\omega) = \frac{N}{\kappa_0} \frac{1}{(1+i\omega\tau_i)}$ and when solvent friction dominates ($\tau_R \gg \tau_i$) to the Rouse model, given by the limiting form, $J_{\Delta R}(\omega) = \frac{2N}{\pi\kappa_0} \tanh\left(\frac{\pi}{2} \sqrt{i\omega\tau_R}\right) / \sqrt{i\omega\tau_R}$, till a critical frequency $1/\tau_i$, when the internal friction of high curvature modes dominates to give single mode relaxation again. The Fluctuation-Dissipation Theorem (FDT)³³, $P(\omega) = -2k_B T J''(\omega)/\omega$ is then used to calculate the

total power spectrum $P(\omega)$ of a RIF polymer combined with a SHO response of the cantilever and cantilever, where $J''(\omega)$ is the imaginary part of the response function $J(\omega)$.

Shown in Fig.4a are the effective monomer elasticity of cellulose and dextran, from the RIF model fits and normalised by contour length. In previous work²⁴ we showed that calculating the elasticity spectrum directly from the numerical derivative of extensible FJC fits, and secondly from the thermal spectroscopy method agree very well. We verify that using the more refined RIF + cantilever model to analyse the PSD, also provides very good agreement. As previous studies have shown^{2-5, 18, 19, 24, 25}, at low force (in these experiments), elasticity is due to the reduction of chain conformational entropy as it approaches its contour length, after which contour length elongation with constant elasticity becomes more favourable. At higher force, however, the minimum in the elasticity spectra for dextran at ~ 1000 pN, which is absent in the cellulose spectrum, marks a clear signal of the conformational transition in the former.

The key advance afforded by using the RIF model in analysing the PSD is the new information about the two sources of dissipation, not distinguished in previous work^{18, 19, 24, 25}; the solvent friction and internal friction of the single biomolecule. We find consistently from the RIF analysis, that solvent friction is very small within the errors of this experiment ($\leq 0.01 \mu\text{gkHz}$). Hence, these chains are ‘short’, as defined by $N \ll \sqrt{\zeta_{i0}/\zeta_{s0}}$ ³⁴, where $N \sim 400$, which indicates that dissipation is dominated by internal friction at high stretch, and explains the success of the spring and dashpot model in previous modelling of the dissipation of dextran^{18, 19, 24, 25}. The internal friction force spectrum itself exhibits non-trivial behaviour as shown by the comparison of cellulose and dextran in Fig.4b. At low force, both polymers show an increasing internal friction with force, followed by a plateau. Crucially, at higher forces, the spectra of cellulose and dextran differ; qualitatively, the minimum in the internal friction force spectrum of dextran at ~ 1000 pN and its absence in cellulose, confirms that source of this change in the friction of dextran is from the chair-boat conformational transition of the glucose ring.

To make this conclusion more concrete we link the features of the experimental elasticity and friction force spectra to the conformational transition in dextran, using a simple model of population dynamics on a discrete 2-state energy landscape, which we show predicts the same viscoelastic signature of simple forced transitions, as seen in Fig.4. The parameters of the discrete 2-state model are as described in Fig.5a, in which we assume populations obeys Boltzmann statistics and dynamics follow activated Arrhenius transition rates. Using an approach similar

to^{35,36}, the effective response of the populations at a frequency ω can be calculated by applying an oscillatory force $f_0 \cos \omega t$ to the energy landscape. The dynamics of the population $p(t)$ in state 1 (say, the short state, so that probability of extended state is $1 - p(t)$) are then described by $\frac{dp}{dt} = -(\lambda_{12}(t) + \lambda_{21}(t))p(t) + \lambda_{21}(t)$, where the rates λ_{12} , λ_{21} vary with time due to the oscillating perturbation of the landscape. In the Brownian linear response limit ($f_0 x \ll k_B T$), there are in-phase and out-of-phase oscillating solutions to this differential equation, such that the extensional response of the monomer is a simple spring and dashpot $J_{12}(\omega) = \frac{1}{\kappa_{12} + i\zeta_{12}\omega}$, for which we identify the effective elasticity and friction as:

$$\kappa_{12}(F) = \frac{k_B T}{(\Delta x)^2} \frac{1}{p_0(F)(1 - p_0(F))}, \quad (3)$$

$$\zeta_{12}(F) = \frac{k_B T}{(\Delta x)^2} (\tau_{12}(F) + \tau_{21}(F)), \quad (4)$$

and where $p_0(F) = (1 + e^{-\beta \Delta G(F)})^{-1}$ is the equilibrium Boltzmann probability for the short state. In addition, τ_{12} is the forward hopping time between states and τ_{21} is the corresponding backward time, where in general $\tau_{ij} = \tau_0 e^{\beta \Delta G_{ij}^\ddagger(F)}$, with $\beta = 1/k_B T$, ΔG_{ij}^\ddagger the free energy barriers for interconversion and $\tau_0 = 2\pi\zeta_b/\kappa_b$ is a prefactor that arises from mapping the Kramers' first passage problem on a continuous free energy landscape³⁷ $G(x)$ to a discrete description (Fig.5a), where ζ_b and κ_b are the effective friction and curvature of the barrier.

Plotting these (Fig.5b&c - on a natural logarithmic scale to emphasise their exponential nature) we see a characteristic minimum in both the elasticity and internal friction force spectra. In the former case, it is clear that the source of the elasticity is *entropic* in nature and not enthalpic as has been previously asserted³; force controls the shape of the energy landscape or the relative populations of monomers in short or extended states and hence, the effective 'size of box' that the monomer can explore. So Eq.(3) is an expression of the equipartition theorem $\kappa = k_B T / \langle \Delta b^2 \rangle$, where $\langle \Delta b^2 \rangle$ is the mean square fluctuations of the monomer; in Fig.5b at low force, $\Delta G(F)$ is large and positive, hence monomers are confined to the short state, fluctuations $\langle \Delta b^2 \rangle$ are small and the effective stiffness is large. As force decreases the energy difference, populations spread across the two states and the effective size of the box $\langle \Delta b^2 \rangle$ increases, causing the stiffness to decrease (exponentially). The stiffness subsequently passes through a minimum when $\Delta G(F) = 0$

and $\langle \Delta b^2 \rangle$ is maximum, corresponding to a state of maximum entropy, when the probabilities to be in either of the states are equal. On further increase of force, $\Delta G(F)$ becomes negative and monomers become increasingly confined to the extended state ($\langle \Delta b^2 \rangle$ decreasing) and the stiffness increases exponentially. It is simple to see that the elasticity is purely entropic, since any enthalpic contributions to the free energy difference ΔG_0 can contribute only linearly to the free energy as the extension of the monomer is increased. Thus, the molecular elasticity of a monomer is defined by its entropy on a discrete energy landscape.

Eq.(4) predicts that the internal friction for a 2-state landscape is proportional to the sum of the times to interconvert from state 1 to 2 and back, from state 2 to 1. Applying a force to the monomers changes the activation barriers to interconversion, which changes the average time to interconvert and thus ultimately, the internal friction. Fig.5c shows schematically how the internal friction should vary with force in a discrete two-state landscape. As force lowers the barrier $\Delta G_{12}^\ddagger(F)$ of interconverting from 1 \rightarrow 2, the internal friction should decrease, passing through a minimum when the barriers on either side are approximately equal (when $x_1 = x_2$ this occurs at exactly $\Delta G_{12}^\ddagger = \Delta G_{21}^\ddagger$) and then increase again at high force as the barrier for the reverse transition (ΔG_{21}^\ddagger) and hence τ_{21} , becomes large. It is interesting to note that, whilst the hopping time passes through a minimum, the corresponding relaxation time $\tau = \tau_{12}^{-1} + \tau_{21}^{-1}$ must pass through a maximum, since relaxation is dominated by the *smallest* barrier. Hence, on average fluctuations away from equilibrium occur on a hopping timescale $\tau^* \sim \tau_{12} + \tau_{21}$, whilst relaxation back to equilibrium occurs on the timescale τ . We see Eq.(4), is a microscopic fluctuation-dissipation relation for a discrete bistable landscape, that links friction to the timescale for fluctuations due to activated barrier-hopping.

Useful information about the position of the transition state can also be obtained by analysing the relative positions of the minima in the elasticity and internal friction spectra. The difference in the forces at which the minima occur ΔF , can be found from the derivatives of Eq.(3) and Eq.(4):

$$\Delta F = \frac{k_B T}{\Delta x} \ln \left(\frac{x_1}{x_2} \right), \quad (5)$$

and thus provides information on the relative position of the transition state, x_1 or x_2 ($\Delta x = x_1 + x_2$).

The results of this population dynamics model, thus provide a simple way to understand the minima in the elasticity and internal friction spectra, in terms of entropy and barrier-hopping. However, to understand the entire force regime ($\sim 100 \rightarrow 1500\text{pN}$), in addition to the viscoelasticity of the 2-state conformational transition, we need to include the physics of the chain at low and intermediate forces, before the critical force at which the conformational transition occurs. At low force we use a Frictional Freely Jointed Chain (FFJC) model (Appendix) of rods interconnected with joints with constant friction ζ_θ to give an elasticity $\kappa_{FFJC}(F) = \frac{F^2}{k_B T}$ and an internal friction that increases linearly with force, $\zeta_{FFJC}(F) = \frac{\zeta_\theta}{2k_b T b} F$, which are both valid at high stretch ($F \gg k_B T/b \sim 4\text{pN}$ for $b \sim 1\text{nm}$). At intermediate force we account for the local viscoelasticity of stretching a dextran monomer in the short or extended states, using constant elasticities κ_1 , κ_2 , and internal frictions ζ_1 , ζ_2 , respectively. We assume that these processes add mechanically in series, since they provide independent and additive extensions to the overall chain length (see Methods).

Fitting to the elasticity force spectra of cellulose and dextran (normalised by contour length), we find excellent agreement as shown in Fig.4a, where the solid line represents the full elasticity Eq.(7) generated using the average of the parameters determined over a number of single molecule experiments (Cellulose: $\kappa_1 = 36000 \pm 18000 \text{ pN/nm}$, $b = 1 \pm 0.5\text{nm}$; Dextran: $\Delta G_0 = 16.5 \pm 0.4k_B T$, $\Delta x = 0.066 \pm 0.005\text{nm}$, $\kappa_1 = 10000 \pm 1000\text{pN/nm}$, $\kappa_2 = 39000 \pm 2000\text{pN/nm}$, $b = 0.63 \pm 0.02\text{nm}$). These values agree well with the literature^{2,3,5,38}. With confidence we can describe the whole elastic force spectra for both cellulose and dextran; at low force (below 800pN) stiffness increases as entropy is lost due to the orientation of monomers along the line of force and finally reaches a plateau representing a constant stiffness due to the enthalpy of stretching the bonds comprising the glucose ring. However, the response of dextran differs dramatically at higher force as the more extended state becomes thermodynamically favourable. Within the framework of the 2-state model presented, the subsequent decrease in stiffness can be understood since it becomes more *entropically* favourable for the chain to elongate. Interestingly, in the elasticity spectrum of dextran, at around 400-500pN, the model slightly, but consistently, underpredicts the elasticity below this force and overpredicts it above this force. This plateau may be explained by the entropic elasticity of other internal states, possibly the C5-C6 bond rotation in dextran^{2,39}.

In performing fits to the internal friction spectra, all elastic parameters are constrained to values obtained from fits to the elasticity spectra (see Methods). Below we discuss quantitative values of each of these friction processes separately, even though actual fits were performed globally

across the whole force range.

Firstly, we examine the effective internal friction associated with stretching the glucose monomers in their various conformations. For cellulose, we find $\zeta_1 = 110 \pm 50 \mu\text{gkHz}$ and for dextran, $\zeta_1 = 25 \pm 10 \mu\text{gkHz}$ and $\zeta_2 = 120 \pm 50 \mu\text{gkHz}$, for the short and extended states, respectively. Strikingly, these numbers are roughly 7 orders of magnitude larger than the friction expected due to solvent ($\zeta = 6\pi\eta b \sim 10^{-5} \mu\text{gkHz}$ for $b \sim 1\text{nm}$). The most plausible source for such a high local effective friction is roughness in the free energy landscape. A model of dynamics on a rough Gaussian landscape with RMS energy fluctuations ε^{40} predicts a sensitive enhancement to the effective friction constant $\zeta^* = \zeta \exp(\varepsilon/k_B T)^2$, giving an effective roughness for stretching cellulose and dextran as $\varepsilon \approx 4k_B T$. For comparison, recent constant loading rate experiments⁴¹ on the protein imp- β , using theoretical results in⁴² suggest a Gaussian roughness of order $\varepsilon \approx 5.7k_B T$. In the case of these polysaccharides, this roughness may arise from the many sub-states separated by barriers that must be traversed in stretching the monomers; for example, there are many conformations of a glucose ring, (in total 14 canonical chair, boat and twist-boat conformations, separated by 12 half-chair and 12 envelope conformational transition states^{26,43}), which will contribute to extension and may become more or less favourable under tension. In addition, the hydroxyl groups of glucose give rise to the possibility of intra and intermonomer hydrogen bonding, as well differing degrees of solvent accessibility. Such states are particularly suggested by slow undulations in the elasticity and internal friction spectra of cellulose for forces greater than 1000 pN.

At low force, we see a similar picture for the ‘joint’ friction of the FFJC model, obtaining values of the order $\zeta_\theta \sim 1 \mu\text{gnm}^2\text{kHz}$ (cellulose: $\zeta_\theta = 0.9 \pm 0.7 \mu\text{gnm}^2\text{kHz}$; whilst for dextran errors from fits suggest $\zeta_\theta < 1.2 \mu\text{gnm}^2\text{kHz}$). These numbers are roughly 6 orders magnitude greater than the friction of a rod of length b rotating in a solvent ($\pi\eta b^3/4 \sim 10^{-6} \mu\text{gnm}^2\text{kHz}$). We can again appeal to an underlying molecular explanation, where joint friction is due to hopping between dihedral angular states, with an average hopping time of $\tau_{hop} \sim \zeta_\theta/k_B T \approx 0.25\text{msec}$. Again, these very slow dynamics are suggestive of an underlying roughness to the rotational free energy ($\varepsilon \approx 3.7k_B T$, where $\zeta^*/\zeta \sim 10^6$).

In the case of dextran, the marked decrease in internal friction around $\sim 1000\text{pN}$, contains information on the dynamics of interconversion between the short and extended states, for which Eq.(4) provides a simple model. In principle, fitting to the internal friction spectra would determine

the position of the barrier x_1 (with constraint $x_2 = \Delta x - x_1$) and the zero-force interconversion times $\tau_{12}(F = 0)$ and $\tau_{21}(F = 0)$ (measurements at different temperatures could in principle, determine the free energy barriers for conversion in each direction). However, although we find very good fits around the transition region, they are underdetermined, due to the low frequency restriction of the data.

To constrain our fits further, we use Eq.(5). Inspecting Fig.4a&b (solid squares), indicates that $\Delta F \approx 0 \pm 100\text{pN}$, given that the spacing of points in the spectra is approximately 100pN. However, negative values of ΔF imply from Eq.(5) a transition state that is closer to the short state than long ($\frac{x_1}{x_2} < 1$), which is not feasible on geometric grounds, given that its curvature is roughly four times smaller than the extended state ($\frac{\kappa_1}{\kappa_2} \approx \frac{1}{4}$) and that the forward free energy barrier must obey $\Delta G_{012}^\ddagger > \Delta G_0 (= 16.5k_B T)$. Hence, a reasonable assumption is that $0 < \Delta F < 100\text{pN}$, implying a position of the transition state in the region $0.033 < x_1 < 0.053\text{nm}$. Fitting to the friction spectra, so as to satisfy this constraint on x_1 , we find $1\text{ns} < \tau_{21}(0) < 100\text{ns}$ and $0.01\text{s} < \tau_{12}(0) < 1\text{s}$ (see Methods). From Kramers' theory³⁷ of activated diffusive barrier crossing, the exponential prefactors of these times are related to the curvature κ_b and friction ζ_b of the barrier, which when mapped onto a discrete landscape is given by $\tau_0 = 2\pi\zeta_b/\kappa_b$. Thus, given an order of magnitude estimate of the barrier friction $\zeta_b \sim \frac{1}{2}(\zeta_1 + \zeta_2) \approx 70\mu\text{gkHz}$ and that $\tau_0 < \tau_{21}(0)$, we find that the barrier must be very sharp; given by the following approximate bound, $\kappa_b > 10^6\text{pN/nm}$. Fig.6 shows a graphical to-scale reconstruction of the free energy landscape based on the parameters extracted from the modelling of the viscoelastic force spectra of dextran.

In summary, we have shown how macroscopic ideas of elasticity and friction can be extended to the study of the energy landscape of conformational transitions. Eq.3 and Eq.4 are in essence microscopic equivalents of the equipartition theorem and the diffusive fluctuation-dissipation relation, where the spatial and temporal properties of the fluctuations are determined by the shape of the energy landscape, which in turn determine its effective elasticity and friction. In the case of dextran, applying tension to its energy landscape, drives an entropic transition, where elasticity and friction decreases as the populations become more spread and barriers are lowered. These ideas are of wide relevance; from applications to the field of molecular nanotechnology, where microscopic processes of elasticity and internal friction may guide and constrain engineering design, to understanding fundamental processes of molecular biology, such as the study of internal transitions in biomolecules, including the action of molecular motors, allosteric signalling, force-sensing between cells, stretching transitions in DNA and RNA, and emerging data on elasticity and

dissipation from the fluctuations of a refolding protein.

References

1. Evans, E. & Ritchie, K. Dynamic strength of molecular adhesion bonds. *Biophysical Journal* **72**, 1541–1555 (1997).
2. Rief, M., Oesterhelt, F., Heymann, B. & Gaub, H. Single molecule force spectroscopy on polysaccharides by atomic force microscopy. *Science* **275**, 1295–1297 (1997).
3. Marszalek, P., Oberhauser, A., Pang, Y. & Fernandez, J. Polysaccharide elasticity governed by chair-boat transitions of the glucopyranose ring. *Nature* **396**, 661–664 (1998).
4. Li, H., Rief, M., Oesterhelt, F. & Gaub, H. Single-molecule force spectroscopy on xanthan by AFM. *Adv. Mater.* **10**, 316–319 (1998).
5. Marszalek, P., Li, H., Oberhauser, A. & Fernandez, J. Chair-boat transitions in single polysaccharide molecules observed with force-ramp AFM. *Proc. Natl. Acad. Sci. USA* **99**, 4278–4283 (2002).
6. Cluzel, P. *et al.* DNA: an extensible molecule. *Science* **271**, 792–794 (1996).
7. Smith, S. B., Cui, Y. & Bustamante, C. Overstretching B-DNA: the elastic response of individual double-stranded and single-stranded DNA molecules. *Science* **271**, 795–799 (1996).
8. Rief, M., Clausen-Schaumann, H. & Gaub, H. Sequence-dependent mechanics of single DNA molecules. *Nat. Struct. Biol.* **6**, 346–349 (1999).
9. Rief, M., Gautel, M., Oesterhelt, F., Fernandez, J. & Gaub, H. Reversible unfolding of individual titin immunoglobulin domains by AFM. *Science* **276**, 1109–1112 (1997).
10. Mitsui, K., Hara, M. & Ikai, A. Mechanical unfolding of α 2-macroglobulin molecules with atomic force microscope. *FEBS Lett.* **385**, 29–33 (1996).
11. Li, H. *et al.* Reverse engineering of the giant muscle protein titin. *Nature* **418**, 998–1002 (2002).
12. Brockwell, D. J. *et al.* Pulling geometry defines the mechanical resistance of a beta-sheet protein. *Nat Struct Biol* **10**, 731–737 (2003). URL <http://dx.doi.org/10.1038/nsb968>.

13. Carrion-Vazquez, M. *et al.* The mechanical stability of ubiquitin is linkage dependent. *Nat. Struct. Biol.* **10**, 738–743 (2003).
14. Williams, P. *et al.* Hidden complexity in the mechanical properties of titin. *Nature* **422**, 446–449 (2003).
15. Wand, A. J. Dynamic activation of protein function: a view emerging from NMR spectroscopy. *Nat Struct Biol* **8**, 926–931 (2001). URL <http://dx.doi.org/10.1038/nsb1101-926>.
16. Rief, M., Fernandez, J. & Gaub, H. Elastically coupled two-level systems as a model for biopolymer extensibility. *Physical Review Letters* **81**, 4764–4767 (1998).
17. McLeish, T. C. B. Tube theory of entangled polymer dynamics. *Adv. Phys.* **51**, 1379–1527 (2002).
18. Humphris, A., Tamayo, J. & Miles, M. Active quality factor control in liquids for force spectroscopy. *Langmuir* **16**, 7891–7894 (2000).
19. Humphris, A., Antognozzi, M., McMaster, T. & Miles, M. Transverse dynamic force spectroscopy: A novel approach to determining the complex stiffness of a single molecule. *Langmuir* **18**, 1729–1733 (2002).
20. Janovjak, H., Miller, D. J. & Humphris, A. D. L. Molecular force modulation spectroscopy revealing the dynamic response of single bacteriorhodopsins. *Biophys J* **88**, 1423–1431 (2005). URL <http://dx.doi.org/10.1529/biophysj.104.052746>.
21. Higgins, M. J., Sader, J. E. & Jarvis, S. P. Frequency modulation AFM reveals individual intermediates associated with each unfolded I27 titin domain. *Biophys J* (2005). URL <http://dx.doi.org/10.1529/biophysj.105.066571>.
22. Okajima, T., Arakawa, H., Alam, M. T., Sekiguchi, H. & Ikai, A. Dynamics of a partially stretched protein molecule studied using an atomic force microscope. *Biophys Chem* **107**, 51–61 (2004). URL <http://dx.doi.org/10.1016/j.bpc.2003.08.006>.
23. Mitsui, K., Nakajima, K., Arakawa, H., Hara, M. & Ikai, A. Dynamic measurement of single protein's mechanical properties. *Biochem Biophys Res Commun* **272**, 55–63 (2000).

24. Kawakami, M. *et al.* Viscoelastic properties of single polysaccharide molecules determined by analysis of thermally driven oscillations of an atomic force microscope cantilever. *Langmuir* **401**, 400–403 (2004).
25. Kawakami, M. *et al.* Viscoelastic measurements of single molecules on a millisecond time scale by magnetically driven oscillation of an atomic force microscope cantilever. *Langmuir* **21**, 4765–4772 (2005).
26. Stoddart, J. *Stereochemistry of Carbohydrates* (Wiley-Interscience, 1971).
27. Marszalek, P. *et al.* Atomic levers control pyranose ring conformations. *Proc. Natl. Acad. Sci. USA* **96**, 7894–7898 (1999).
28. Pugh, D. & MacInnes, D. Cooperative mode interpretation of molecular weight independence of acoustic and dielectric absorption in polymer solutions. *Chemical Physics Letters* **34**, 139–142 (1975).
29. McInnes, D. & North, A. Dynamics of polymer molecules: a comparison of strongly coupled correlated (internal viscosity) and non-correlated (local mode) models for molecular weight independent conformational relaxation. *Polymer* **18**, 505–508 (1977).
30. Rouse, P. A theory of linear viscoelastic properties of dilute solutions of coupling polymers. *J. Chem. Phys.* **21**, 1272–1280 (1953).
31. Doi, M. *Introduction to Polymer Physics* (Oxford University Press, 1995).
32. Zimm, B. *J. Chem. Phys.* **24**, 269 (1956).
33. Chaiken, P. & Lubensky, T. *Principles of Condensed Matter Physics* (Cambridge University Press, 1995).
34. de Gennes, P. G. *Scaling Concepts in Polymer Physics* (Cornell University Press, 1985).
35. McNamara & Wiesenfeld. Theory of stochastic resonance. *Physical Review. A* **39**, 4854–4869 (1989). URL http://prola.aps.org/abstract/PRA/v39/i9/p4854_{_}1.
36. Braun, O. & Seifert, U. Periodically driven stochastic un- and refolding transitions of biopolymers. *Europhys. Lett.* **68**, 746–752 (2004). URL <http://dx.doi.org/10.1209/epl/i2004-10279-1>.

37. Kramers, H. Brownian motion in a field of force and the diffusion model of chemical reactions. *Physica* **7**, 284–304 (1940).
38. Janshoff, A., Neitzert, M., Oberdörfer, Y. & Fuchs, H. Force spectroscopy of molecular systems—single molecule spectroscopy of polymers and biomolecules. *Angew. Chem. Int. Ed.* **39**, 3212–3237 (2000).
39. Lee, G., Nowak, W., Jaroniec, J., Zhang, Q. & Marszalek, P. E. Molecular dynamics simulations of forced conformational transitions in 1,6-linked polysaccharides. *Biophys. J.* **87**, 1456–1465 (2004).
40. Zwanzig, R. Diffusion in a rough potential. *Proc. Natl. Acad. Sci.* **85**, 2029–2030 (1988).
41. Nevo, R., Brunfeld, V., Kapon, R., Hinterdorfer, P. & Reich, Z. Direct measurement of protein energy landscape roughness. *EMBO Reports* **6**, 482–486 (2005).
42. Hyeon, C. & Thirumalai, D. Can energy landscape roughness of proteins and RNA be measured by using mechanical unfolding experiments. *Proc. Natl. Acad. Sci.* **100**, 10249–10253 (2003).
43. Ionescu, A. R., Bérces, A., Zgierski, M. Z., Whitfield, D. M. & Nukada, T. Conformational pathways of saturated six-membered rings. A static and dynamical density functional study. *J. Phys. Chem. A* **109**, 8096–8105 (2005).
44. O’Donoghue, P. & Luthey-Schulten, Z. A. Barriers to forced transitions in polysaccharides. *J. Phys. Chem. B* **104**, 10398–10405 (2000).

Methods

Experimental Materials & Methods The protocol used for thermal force-clamp spectroscopy is as described in²⁴, we summarise the procedure here. The first part of the experiment follows conventional force-spectroscopy protocol, where the cantilever is pressed into a polysaccharide monolayer with a force ~ 10 nN for ~ 1 s, after which it is retracted from the substrate at a constant speed. When a pre-determined force set-point is reached, the force-clamp protocol is initiated, which involves either reducing force in discrete steps of ~ 100 pN and being held for ~ 3 s, or reducing force slowly and continuously at ~ 8 pN/s. In some measurements we have used this latter continuous approach, however, both procedures produce the same results within the

errors of each method (not shown). In either method the force is controlled using a proportional-integral-derivative (PID) feedback loop with a response time of ~ 10 ms, whereby the cantilever substrate separation is adjusted to maintain a certain cantilever deflection. A response time of ~ 10 ms means the feedback loop cannot respond to fluctuations faster than 10 ms. Thus, for frequencies greater than ~ 0.1 kHz, an average force F is maintained. After the force-clamp phase, the cantilever is again retracted from the substrate at a constant speed, till at some critical force the polymer detaches. Immediately after detachment, the PSD of the free cantilever is recorded as the cantilever is brought towards the substrate in 30 nm steps. These free cantilever PSD are then fit using a simple harmonic oscillator model (SHO), $P_c(\omega) = \frac{2k_B T \zeta_c}{(\kappa_c - m_c \omega^2)^2 + \zeta_c^2 \omega^2}$, obtaining the cantilever effective stiffness κ_c , friction constant ζ_c and mass m_c . These parameters then serve as constraints in the curve fits to the power spectra of the cantilever/molecule system.

To extract the elasticity, internal and solvent friction as functions of force, we treat the force clamp experiment as two linear system elements in parallel, since the change in extension of the polymer and cantilever are the same at their point of contact. It can be shown (Appendix), that for a system in parallel the total dynamic compliance of the system $J_T(\omega)$ is given by

$$J_T(\omega) = \frac{J_X(\omega)J_{\Delta R}(\omega)}{J_X(\omega) + J_{\Delta R}(\omega)}, \quad (6)$$

where $J_X(\omega)$ is the dynamic compliance of the cantilever, for which we use a SHO model ($J_X(\omega) = (\kappa - m\omega^2 + i\zeta\omega)^{-1}$). This is just the frequency-dependent extension of the parallel addition that arises naturally in our experiment. We then use the fluctuation dissipation theorem (FDT) $P(\omega) = -2k_B T J''(\omega)/\omega$ ³³ (J'' represents the imaginary part of the complex function J) and Eq.(2) & Eq.(6) to calculate the total power spectrum of the cantilever + RIF polymer. This enables measurement of the elasticity, internal friction and solvent friction as functions of force, for example, as shown by the RIF model fits to the power spectra of cellulose in Fig.3. In fitting the PSDs to the RIF+cantilever model, we constrain the chain solvent friction to be between $0 < \zeta_s < 0.1$ μgkHz , since a reasonable estimate of the solvent friction is given by $6\pi\eta L_c \approx 4 \times 10^{-3}$ μgkHz , where the contour length $L_c \approx 200$ nm, is the typical contour length of molecules in the experiment, representing the maximum effective hydrodynamic radius of the chain³⁴.

Fitting to Elasticity and Internal Friction. In both the elasticity and internal friction force spectra, there are a number of different physical processes that underly the observed behaviour. A reasonable assumption is that the noise on each physical processes is uncorrelated, so that the total

power spectrum is the sum of the power spectra of each process. In the low frequency regime of the experiments ($\omega\tau \ll 1$), the rules for summing the elasticity and frictions of the different processes are then:

$$\kappa(F) = \left(\kappa_{FJC}^{-1}(F) + \kappa_{12}^{-1}(F) + p_0(F)\kappa_1^{-1} + (1 - p_0(F))\kappa_2^{-1} \right)^{-1}, \quad (7)$$

$$\zeta(F) = \kappa^2(F) \left(\frac{\zeta_{FJC}(F)}{\kappa_{FJC}^2(F)} + \frac{\zeta_{12}(F)}{\kappa_{12}^2(F)} + p_0(F) \frac{\zeta_1}{\kappa_1^2} + (1 - p_0(F)) \frac{\zeta_2}{\kappa_2^2} \right), \quad (8)$$

where importantly, the bond elasticities of the short and extended states are weighted by the probability to be in those states at a given force, where $p_0(F) = (1 + e^{-\beta\Delta G(F)})^{-1}$. In fitting to the internal friction force spectra, we use the parameters extracted from fitting to the elasticity spectra as a constraint to the fits. Through trial and error with fits with different fixed values of $\tau_{21}(0)$, we found the values of the zero-force backward hopping time that correspond to the bound calculated on x_1 in the main text. We checked that the values of $\tau_{12}(0)$ also determined from the fits, were consistent with detailed balance ($\tau_{12}(0)/\tau_{21}(0) = e^{\beta\Delta G_0}$).

Acknowledgements We thank EPSRC (UK) for financial support. M.K. was a JSPS Visiting Research Fellow and is now supported by the EPSRC. T.C.B.M. is an EPSRC Advanced Fellow. We thank Igor Neelov and Peter Olmsted, School of Physics & Astronomy, University of Leeds and Stuart Warriner, School of Chemistry, University of Leeds, for fruitful discussions. We are particularly grateful to Sheena Radford, Astbury Centre for Structural Molecular Biology, University of Leeds, for many useful and stimulating discussions.

Correspondence and requests for materials should be addressed to T.C.B.M.(email:t.c.b.mcleish@leeds.ac.uk).

Figure 1. Structure of dextran and cellulose. (a) Simplified diagram of the molecular structure of dextran, which is an α -(1 \rightarrow 6) linked polysaccharide of glucose, where the monomer length is defined by the distance between adjacent non-ring oxygens on the backbone, as shown schematically. The α linkage at C1 is axial in the lowest energy 4C_1 chair conformation²⁶ (above), which under application of a tensile force-field promotes one of a number of more elongated *boat* or *skew-boat* conformations, of which the ${}^{1,4}B$ is shown (below)^{3,26,43,44}. The increased length Δx gives rise to a plateau in force-extension measurements (Appendix Figure 7) as the more elongated boat-like conformations are populated under increasing force. (b) Cellulose on the other hand is

a β -(1 \rightarrow 4) linked polysaccharide of glucose, whose equatorial linkage at C1 in the chair state, means the monomer is already near maximum elongation and its force-extension behaviour follows simple polymer elasticity models due to reduction of chain entropy at high stretch (Appendix Figure 7).

Figure 2. Force-clamp thermal noise spectroscopy. (a) Schematic diagram of the experimental setup for thermal noise spectroscopy. (b)&(c) show the force clamp protocol used: (b) typical experimental force-extension traces showing a retract, approach and retract cycle, using dextran as the sample polymer, where the traces have been offset for clarity. The characteristic shape of the final curve (curve 3), which in the case of dextran exhibits a shoulder indicative of the well-known conformational transition in dextran², confirms that only a single molecule was attached. (c) experimental force-time trace, where the numbers and colours correspond to the same sequence in (b). The force-clamp phase (phase 2) lasts for a total of 42 seconds, where the dextran polymer is held for 3 seconds at each of 14 discrete forces (the initial and final extensions, phases 1 & 3, are shown on an expanded time scale).

Figure 3. Force dependent PSD of single molecule of cellulose. Comparison of the PSD of fluctuations of cantilever tip, when free (black circles) and with a single cellulose molecule attached, held with forces of 320 pN (green), 620 pN (purple) and 920 pN (red). The solid lines correspond to fits using either a simple harmonic oscillator model for the cantilever (black), or the RIF model of the biopolymer combined with the cantilever (green, purple and red solid lines) described by Eq.(2) & Eq.(6).

Figure 4. Viscoelastic force spectrum of cellulose and dextran. (a) Elasticity force spectrum and (b) internal friction force spectrum multiplied by contour length of each molecule L_c (giving the inverses of the compliance and mobility per unit length) for cellulose (solid diamonds) and dextran (solid squares, where L_c is obtained from FJC fits to their respective force-extension traces (Appendix Figure 7)). Data points represent measurements using thermal force clamp spectroscopy, where different colours represent separate single molecules. The solid lines represent curves generated using the full elasticity (a) and internal friction (b) expressions given in Eq.(7) & Eq.(8), using the average of the parameters determined over all of single molecule experiments (see main text), apart from $\zeta_\theta = 0.6\mu\text{g}\text{nm}^2\text{kHz}$ (half the upper bound in the main text) and 2-state internal friction parameters derived in the text consistent with a fixed zero-force backward interconversion time $\tau_{21}(0) = 100\text{ns}$ (i.e. $\Delta x_1 = 0.053\text{nm}$, $\tau_{12}(0) = 1\text{s}$). Horizontal error bars represent an ap-

proximate 10% systematic error between experiments in determining the true force scale, through errors in measuring cantilever elasticity and cantilever deflection sensitivity. Vertical error bars represent errors from the fits to the PSDs.

Figure 5. Viscoelastic Force Spectrum on a discrete bistable landscape. (a) Schematic diagram of the discrete free energy landscape used to calculate the elasticity and internal friction force spectra (Eq.(3) & Eq.(4)). (b) Elasticity force spectrum on a discrete 2-state landscape; force controls free energy difference $\Delta G(F) = \Delta G_0 - F\Delta x_{12}$ and hence spread $\langle \Delta b^2 \rangle$ and elasticity $\kappa_{12}(F) = k_B T / \langle \Delta b^2 \rangle$. Elasticity is entropic in nature as elasticity decreases in direction of increasing entropy of monomers. (c) Internal friction force spectrum for a discrete 2-state landscape; force controls activation barrier heights ($\Delta G_{12}^\ddagger(F) = \Delta G_{012}^\ddagger - F\Delta x_1$, $\Delta G_{21}^\ddagger(F) = \Delta G_{021}^\ddagger + F\Delta x_2$), and therefore also the internal friction. Hence, at a given force, internal friction is dominated by the activation barrier that is largest.

Figure 6. To-scale reconstruction of continuous free energy landscape of glucose, based on parameters extracted from theoretical modelling of the viscoelastic force spectra of dextran. Dashed features indicate areas of landscape that are uncertain, for example position of barrier, or information unattainable with current experiments like the activation barrier heights. Barrier curvature shown is $\kappa_b = 10^6$ pN/nm. Grey lines indicate a roughness to the landscape with RMS deviation $\varepsilon \approx 4k_B T$, as a plausible interpretation for significantly enhanced friction of wells. $\Delta G'_0 = \Delta G_0 + k_B T \ln(\sqrt{\kappa_1/\kappa_2}) = (16.5 - \ln 2)k_B T \approx 15.8k_B T$ is the free energy difference between the minima of a continuous landscape, which excludes the entropy of vibrations of the wells.

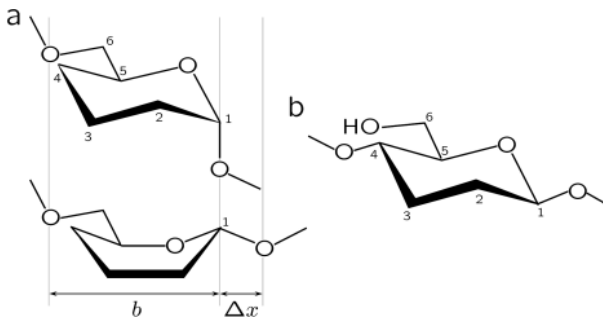


Figure 1

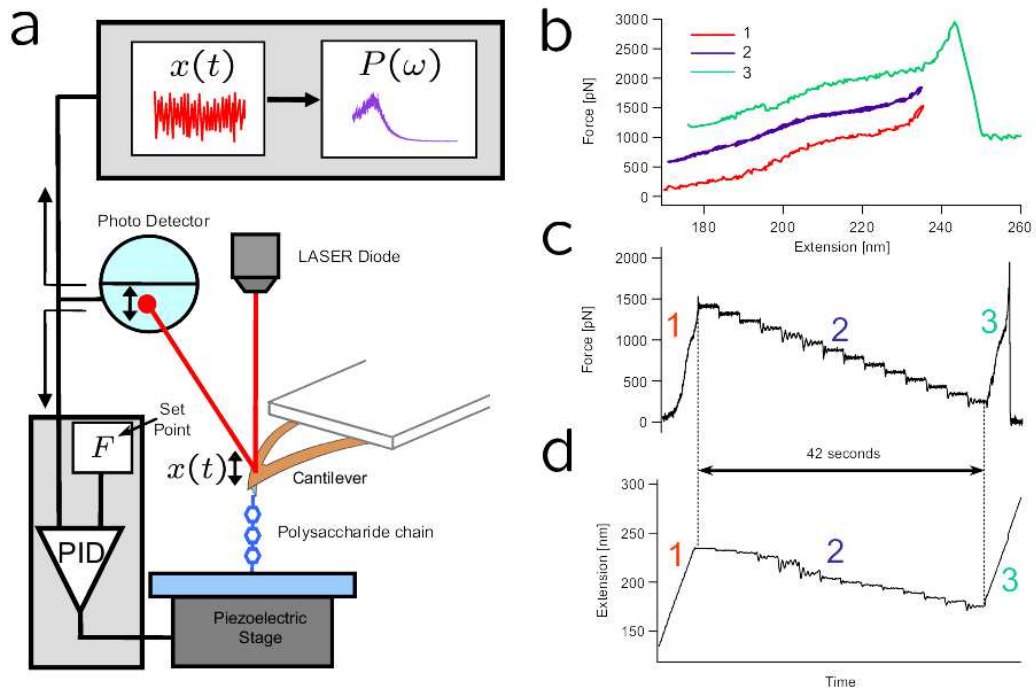


Figure 2

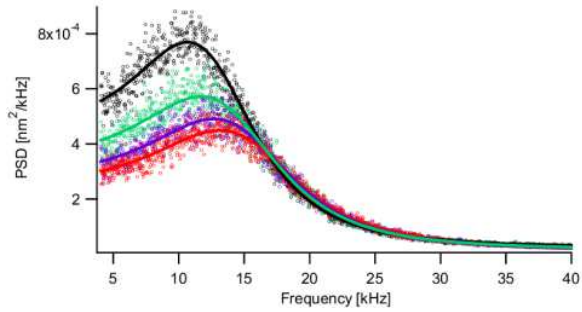


Figure 3

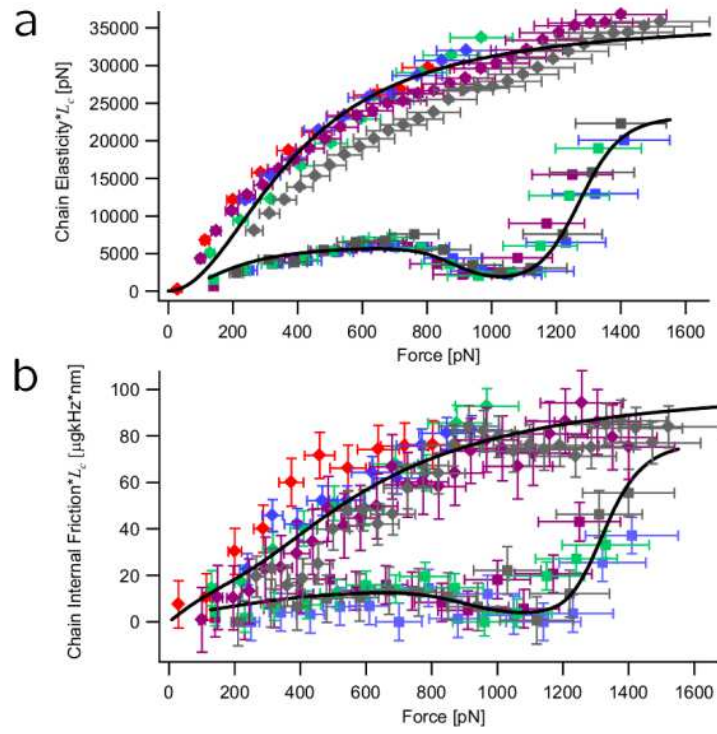


Figure 4

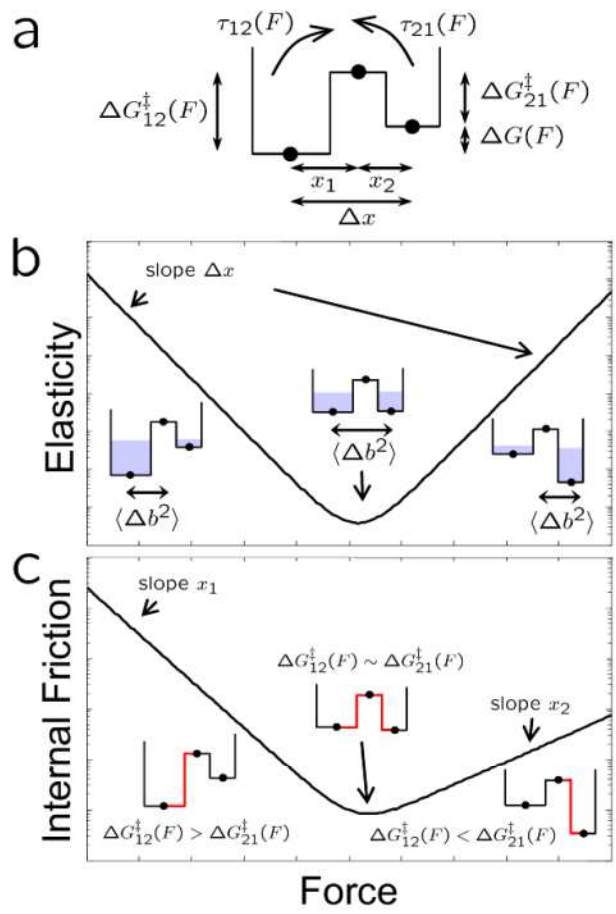


Figure 5

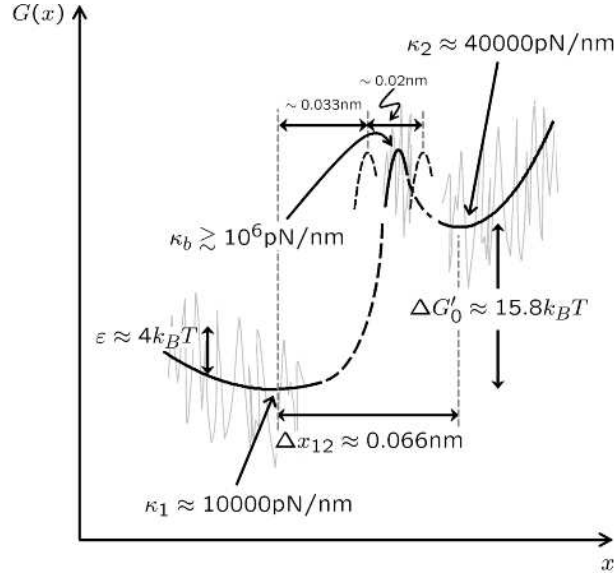


Figure 6

Appendices

Dynamic compliance of parallel system elements Here we derive the total dynamic compliance or response function $J_T(\omega)$ for the cantilever and polymer in parallel, which each have response functions $J_X(\omega)$ and $J_{\Delta R}(\omega)$, respectively. Starting in the time domain, we can write down the solution for the cantilever and polymer motion as:

$$\Delta R(t) = \int_0^t J_{\Delta R}(t-t') \left(\frac{1}{2}F(t') - f(t') \right) dt'$$

$$X(t) = \int_0^t J_X(t-t') \left(\frac{1}{2}F(t') + f(t') \right) dt'$$

where F represents an external force applied to the system and f the internal force that they share according to Newton's 3rd Law. By definition, the Green's response of the whole system is its response to a unit impulse of force, so we let $F(t) = \eta\delta(t)$, where $\delta(t)$ is the Dirac "delta-function" and η the size of impulse. This gives

$$\Delta R(t) = \frac{\eta}{2} J_{\Delta R}(t) - \int_0^t J_{\Delta R}(t-t') f(t') dt'$$

$$X(t) = \frac{\eta}{2} J_X(t) + \int_0^t J_X(t-t') f(t') dt'$$

Taking the Fourier Transform of these (presuming all response functions are zero for $t < 0$) we find

$$\Delta R(\omega) = \frac{\eta}{2} J_{\Delta R}(\omega) - J_{\Delta R}(\omega) f(\omega) \quad (1)$$

$$X(\omega) = \frac{\eta}{2} J_X(\omega) + J_X(\omega) f(\omega) \quad (2)$$

Thus, using the fact that the cantilever and polymer displacements must be the same for all times ($\Delta R(t) = X(t)$), we can solve for the internal force $f(\omega)$:

$$f(\omega) = \frac{\eta J_{\Delta R}(\omega) - J_X(\omega)}{2 J_{\Delta R}(\omega) + J_X(\omega)}$$

this can then be plugged back into Eq.(1) or Eq.(2), to give the total dynamic compliance as the displacement response due to a unit delta function input:

$$J_T(\omega) = \frac{\Delta R(\omega)}{\eta} = \frac{X(\omega)}{\eta} = \frac{J_X(\omega) J_{\Delta R}(\omega)}{J_X(\omega) + J_{\Delta R}(\omega)}$$

Frictional Freely Jointed Chain To model the molecular viscoelasticity of a polymer at forces which are small (approximately, $F < 500\text{pN}$), we develop a Frictional FJC (FFJC) model of rods interconnected with joints with constant friction and calculate the form of $\zeta_{FJC}(F)$. We focus on a

single monomer, assuming that each rod of the FJC is statistically independent, so the stiffness of each rod will add mechanically in series to the stiffness of the whole chain. Typical monomer/rod lengths for polysaccharides are $b \sim 1\text{nm}$, so our experiments are in the regime where $F \gg k_B T/b$ and the elasticity spectrum can be calculated from statistical mechanics as

$$\kappa_{FJC}(F) = \frac{F^2}{k_B T} \quad (3)$$

To model the internal friction of a FJC we again focus on a single monomer/rod in the high force regime and consider that to rotate such a rod there is some friction ζ_θ opposing this motion, which we presume is constant and associated with the internal friction of ‘joints’ between rods. The rotational equation of motion for a segment or rod of length b held under a large tensile force F ($Fb \gg k_B T$) will be

$$\zeta_\theta \dot{\theta}(t) = -Fb\theta \quad (4)$$

Now we consider how these dynamics project onto the line of applied force. The change in projected length of the monomer compared to its actual length will be $\Delta b = b(1 - \cos \theta)$, which in the small angle limit will be:

$$\Delta b \approx \frac{1}{2}b\theta^2 \quad (5)$$

Differentiating Δb , and using Eq.(4) & Eq.(5), we find its equation of motion to be:

$$\dot{\Delta b} = b\theta\dot{\theta} = -\frac{Fb^2\theta^2}{\zeta_\theta} = -\frac{2Fb}{\zeta_\theta}\Delta b$$

This again has an exponentially decaying solution $\Delta b(t) \sim e^{-t/\tau_{FJC}}$, with time constant $\tau_{FJC} = \frac{\zeta_\theta}{2Fb}$. Now $\tau_{FJC} = \zeta_{FJC}/\kappa_{FJC}$ and thus, using Eq.(3), the effective friction along the z direction is

then

$$\zeta_{FJC}(F) = \frac{\zeta_\theta}{2k_b T b} F \quad (6)$$

which predicts a linear increase of the internal friction constant with force, presuming ζ_θ is constant.

Additional Figure

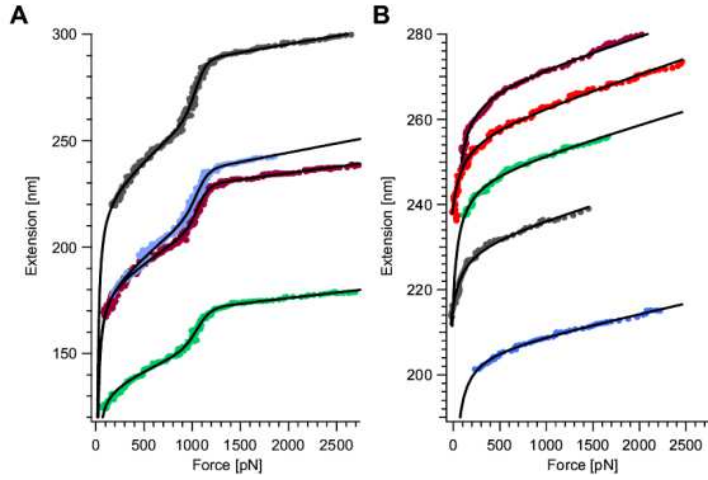


Fig. 7. Extension-Force traces from constant pulling rate experiments for (A) 4 different dextran molecules and (B) 5 different cellulose molecules. Each trace represents the final stage (marked (3) in Fig.2 in main text) of the thermal noise force-clamp spectroscopy protocol from which we determine the contour length L_c . For cellulose we fit the extension as function of force, using a FJC of elastic segments (FJC+), where the chain is characterised by a number of Kuhn segments N_k , which have length b and elasticity κ ⁷, to give a contour length $L_c = N_k b$. For dextran, we assume a Boltzmann weighted sum of the two states, where the monomer lengths in the chair and boat state are represented by different Kuhn segment lengths and elasticity of a FJC+ model:

$$\langle \Delta R(F) \rangle = \frac{N_k}{1 + e^{-\Delta G(F)}} \left(b_1 \mathcal{L}(F b_1) \left(1 + \frac{F}{\kappa_1 b_1} \right) + b_2 \mathcal{L}(F b_2) \left(1 + \frac{F}{\kappa_2 b_2} \right) e^{-\Delta G(F)} \right),$$

where \mathcal{L} is the Langevin function, F is the imposed tension, and $\Delta G(F) = \Delta G_0 - F \Delta x_{12}$, with Δx_{12} being the spatial separation between the two states. Factors of $k_B T$ are dropped for clarity.

For dextran, we assume the contour length is given by $L_c \approx N_k b_1$.